Materials and Design 43 (2013) 393–401

Contents lists available at SciVerse ScienceDirect

Materials and Design

journal homepage: www.elsevier.com/locate/matdes

Constitutive modeling for flow behavior of GCr15 steel under hot compression experiments

Fei Yin [a,b], Lin Hua [a,b,*], Huajie Mao [c], Xinghui Han [a,b]

[a] School of Automotive Engineering, Wuhan University of Technology, Wuhan 430070, China
[b] Hubei Key Laboratory of Advanced Technology of Automotive Parts, Wuhan 430070, China
[c] School of Materials Science and Engineering, Wuhan University of Technology, Wuhan 430070, China

ARTICLE INFO

Article history:
Received 18 May 2012
Accepted 3 July 2012
Available online 20 July 2012

Keywords:
Constitutive model
Steel
Hot deformation
Flow behavior

ABSTRACT

The thermal compressive deformation behavior of GCr15 (AISI-52100), one of the most commonly used bearing steels, was studied on the Gleeble-3500 thermo-simulation system at temperature range of 950–1150 °C and strain rate range of 0.1–10 s^{-1}. According to the experimental results, the stress level decreases with increasing deformation temperature and decreasing strain rate. The peak stresses on the true stress–strain curves suggest that the dynamic softening of GCr15 steel occurs during hot compression tests. To formulate the thermoplastic constitutive equation of GCr15 steel, Arrhenius equation and the Zener–Hollomon parameter in an exponent-type equation were utilized in this paper. In addition, a modified Zener–Hollomon parameter considering the compensation of strain rate during hot compression was employed to improve the prediction accuracy of the developed constitutive equation. Analysis results indicate that the flow stress values predicted by the proposed constitutive model agree well with the experimental values, which confirms the accuracy and reliability of the developed constitutive equation of GCr15 steel.

1. Introduction

With the development of numerical simulation method, Finite Element Method (FEM) has been widely and successfully used to analyze and optimize the materials forming processes such as forging, rolling and extrusion.

Han et al. developed a 3D elastic–plastic dynamic explicit FE model of cold rotary forging under the ABAQUS software environment and they studied the plastic deformation behaviors of cold rotary forging under different contact patterns by utilizing the developed FE simulation model [1]. Deng et al. developed a rigid-plastic finite element (FE) model of cold rotary forging of a 20CrMnTi alloy spur bevel gear. By using the FE model, they optimized the workpiece geometry to achieve a better filling of gear shape and a lower forming load requirement [2]. Zhou et al. explored a 3D elastic–plastic and coupled thermo-mechanical FE model of Radial–axial ring rolling (RARR) by using the dynamic explicit code ABAQUS. Based on the reliable 3D FE model, they investigated the effects of the axial rolls motions and size of rolls on the RARR process. Their research results provide valuable guidelines for the motion control and design of the axial rolls in the actual RARR production [3,4]. Wang et al. developed a three-dimensional coupled thermal–mechanical elastic–plastic FE model of the Vertical Hot Ring Rolling (VHRR) process in ABAQUS/Explicit code. By using the developed FE simulation model, they analyzed the effects of single fixed guide mode and single follow-up guide mode on the ring's dimensional precision during hot ring rolling production, respectively [5].

During the establishment of FE simulation models, constitutive equation of the materials is always used as an input code to simulate the materials deformation behaviors under specified loading conditions [6,7]. The applicable and reliable of the explored FE simulation model is greatly determined by the accuracy of the developed constitutive equation. Researches focusing on formulating the constitutive equation of materials have attracted more and more attention worldwide.

Samantaray et al. analyzed the high temperature flow behavior of various grades of austenitic stainless steels by isothermal hot compression tests. They predicted the flow stress of the materials by applying a modified Zerilli–Armstrong. Research results suggest that the modified Zerilli–Armstrong model could predict the elevated temperature flow behavior of the materials over the entire ranges of strain, strain rate and temperature [8]. Lin et al. studied the compressive deformation behavior of 42CrMo steel by means of the compression test over a practical range of temperatures and strain rates. They formulated a constitutive equation incorporating the effects of temperature, strain rate and work-hardening rate to describe the plastic flow properties of the materials.

* Corresponding author at: School of Automotive Engineering, Wuhan University of Technology, Wuhan 430070, China. Tel.: +86 136 07160833; fax: +86 027 87168391.
E-mail addresses: hualin@whut.edu.cn, hualin_whut@yahoo.cn (L. Hua).

0261-3069/$ - see front matter © 2012 Elsevier Ltd. All rights reserved.
http://dx.doi.org/10.1016/j.matdes.2012.07.009

Research results suggest that the proposed deformation constitutive model could predict the flow stress of 42CrMo steel accurately and precisely [9–11]. They also successfully developed a constitutive model of 42CrMo steel by employing a new material parameter L, which was sensitive to the forming temperature and strain rate [12]. Ding et al. proposed a new time-dependent cyclic visco-plastic constitutive model based on the experimental results of uniaxial time-dependent ratcheting of 6061-T6 aluminum alloy [13]. Han et al. established an adaptive fuzzy-neural network model to model the constitutive relationship of Ti–25V–15Cr–0.2Si alloy during high temperature deformation. Their research results indicate that the fuzzy-neural network was an easy and practical method to optimize deformation process parameters [14].

As one of the most commonly used high-chromium bearing steels, GCr15 steel (AISI-52100) has the characteristics of high wear resistance, corrosion resistance and good dimensional stability. It has been widely used in manufacturing bearing ring, ball screw and other mechanical components. A number of research groups have studied the plastic behavior and material properties of GCr15 steel under specified forming processes by experiment and FE simulation method [15–17]. However, research reports focusing on modeling the constitutive equation of GCr15 steel under hot deformation condition are still unavailable. And a precise thermoplastic constitutive equation for GCr15 steel is still required when establishing the FE model to simulate the thermo-mechanical forming processes of GCr15.

In this paper, the compressive deformation behavior of GCr15 steel was studied and the constitutive equation of the materials was formulated. Gleeble-3500 thermo-simulation system was used to study the thermal compressive deformation behavior of GCr15 steel. The true stress–strain curve for GCr15 steel under different deformation temperatures from 950 °C to 1150 °C with strain rates of $0.1\,s^{-1}$, $1\,s^{-1}$, $5\,s^{-1}$, and $10\,s^{-1}$, was recorded, respectively. According to the experimental results, the stress level decreases with increasing deformation temperature and decreasing strain rate. And the peak stresses on the true stress–strain curves suggest that the dynamic softening of GCr15 steel occurs during hot compression tests. To formulate the thermoplastic constitutive equation of GCr15 steel, Arrhenius equation, commonly used for representing relationship between flow stress and strain rate as well as temperature during hot deformation, was utilized in this paper. And a revised Zener–Hollomon parameter considering the compensation of strain rate during hot compression was employed in this investigation. The flow stress values of GCr15 steel predicted by the developed constitutive model show a good agreement with the experimental results, which confirms the accuracy and reliability of the developed constitutive equation of GCr15 steel.

2. Materials and experiments procedure

A commercial GCr15 high-chromium bearing steel commonly used for manufacturing bearing ring was investigated in this paper. The chemical composition of the GCr15 steel used in this study is shown in Table 1. Hot compression experiments were conducted on the Gleeble-3500 thermo-simulation system as shown in Fig. 1. Fig. 1a is the mechanical part of the Gleeble-3500 thermo-simulation system. And it can be seen in Fig. 1b that the cylindrical specimen with the diameter of 8 mm and height of 12 mm shown in Fig. 2a was clamped between the two compression dies. To decrease the friction between specimens and dies during hot compression, the graphite mixed with machine oil was used

Table 1
Chemical composition of the GCr15 bearing steel used in this study (wt.%).

C	0.96
S	0.006
P	0.013
Mn	0.36
Si	0.19
Cr	1.46
Mo	0.02
Cu	0.06
Ni	0.08
Fe	Balance

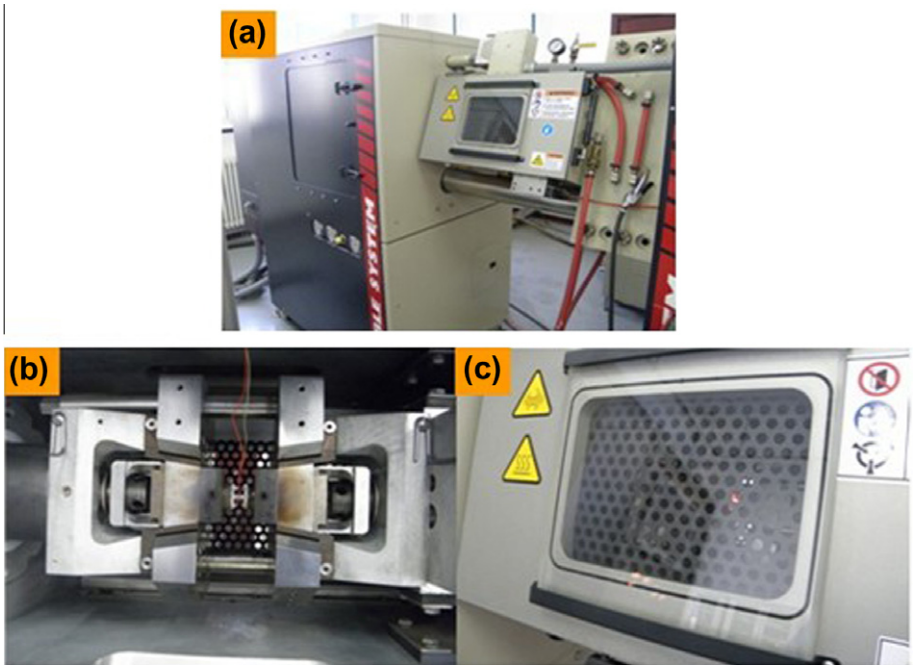

Fig. 1. (a) Gleeble-3500 system; (b) compression area; (c) thermo-compression process.

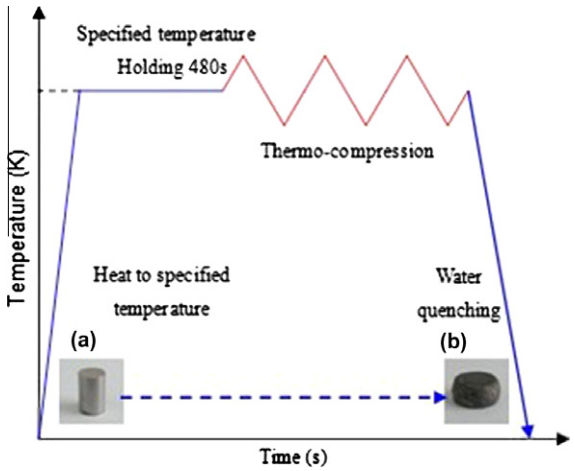

Fig. 2. Experimental procedure and specimen (a) before and (b) after hot compression.

between the flat ends of the specimen and the compression dies [9,11]. The hot compression tests were performed under temperatures of 950 °C, 1000 °C, 1050 °C, 1100 °C, 1150 °C with strain rates of 0.1 s^{-1}, 1 s^{-1}, 5 s^{-1} and 10 s^{-1}. The temperatures of the specimen are controlled by the feedback signals provided by the thermocouples. And Fig. 1c shows the thermo-compression process of the specimen.

The detailed experimental procedure can be seen in Fig. 2. It can be seen in Fig. 2 that the specimen was heated to the specified temperature at the heating rate of 10 °C/s and held for 6 min. Then, the specimen was compressed with a specified strain rate and quenched with water rapidly. The specimen after hot compression can be seen in Fig. 2b and the reduction in height of the specimen after hot compression is 50%.

3. Results and discussion

3.1. True stress–strain curve

Fig. 3 shows the true stress–strain curve for GCr15 steel under different deformation temperature with strain rates of (a) 0.1 s^{-1}; (b) 1 s^{-1}; (c) 5 s^{-1} and (d) 10 s^{-1}. It can be concluded from Fig. 3 that the flow stress decreases with the increase of deformation temperature and decrease of strain rate. And the peak stresses on the true stress–strain curves suggest that the dynamic recrystallization (DRX) and dynamic flow softening of GCr15 steel occurs during hot compression tests.

In addition, the phenomenon of dynamic recrystallization of GCr15 steel during hot compression process was observed by means of electronic microscope. Fig. 4 illustrates the optical micrograph of GCr15 steel after hot compression with strain rate of 1 s^{-1} and temperature of 1000 °C. It can be seen in Fig. 4 that there exists small-sized austenite grain between the average size austenite grains. During hot compression process, the dynamic recrystallization behavior was induced by thermodynamic energy and the recrystallization nuclei were generated and growing. Some recrystallization nuclei have no time to grow as the average austenite gain and the immediate water quenching after the hot compressive

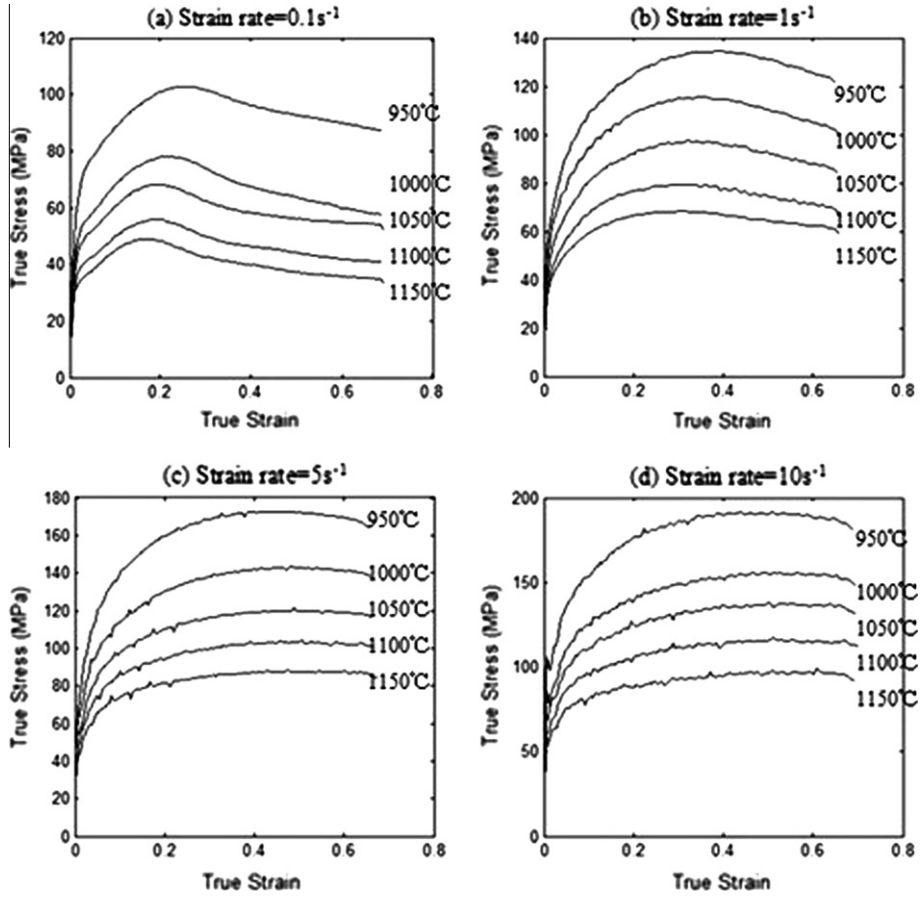

Fig. 3. True stress–strain curves for GCr15 steel under different deformation temperature with strain rates of (a) strain rate = 0.1 s^{-1}; (b) strain rate = 1 s^{-1}; (c) strain rate = 5 s^{-1} and (d) strain rate = 10 s^{-1}.

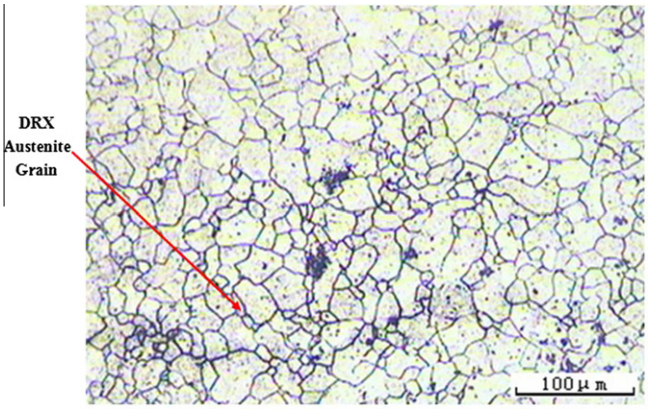

Fig. 4. Optical micrograph of GCr15 steel after hot compression (center area of the specimen).

process stopped the growing process of the austenite gain. Hence, it can be concluded from Fig. 4 that the phenomenon of dynamic recrystallization of GCr15 steel occurs during the hot compression process.

3.2. Modeling of the constitutive equation

To formulate the constitutive equation of the GCr15 steel, the Arrhenius equation which is widely used to describe the relationship between the strain rate, temperature and flow stress was utilized in this study [18,19]. For all stress level, the Arrhenius equation can be formulated as following equation:

$$\dot{\varepsilon} = A \sinh(\alpha\sigma)^n \exp\left(-\frac{Q}{RT}\right) \tag{1}$$

where $\dot{\varepsilon}$ is the strain rate (s^{-1}); R is the universal gas constant (8.31 J $mol^{-1}K^{-1}$); T is the absolute temperature (K); Q is the activation energy of hot deformation (k J mol^{-1}); σ is the true stress (MPa); n is the materials stress index; A and α are the materials constants.

In addition, the effects of the temperature and strain rate on the deformation behaviors can also be formulated by Zener–Hollomon parameter, Z, in an exponent-type equation as shown in following equation:

$$Z = \dot{\varepsilon} \exp\left(\frac{Q}{RT}\right) \tag{2}$$

where Z is the temperature compensation strain rate factor during hot deformation.

By substituting Eq. (1) into Eq. (2) gives Eq. (3). And by solving the Eq. (3), the flow stress can be written as a function of Z parameter as shown in Eq. (4).

$$Z = A[\sinh(\alpha\sigma)]^n \tag{3}$$

$$\sigma = \frac{1}{\alpha} \ln\left\{\left(\frac{Z}{A}\right)^{1/n} + \left[\left(\left(\frac{Z}{A}\right)^{2/n} + 1\right)\right]^{1/2}\right\} \tag{4}$$

3.2.1. Determination of the material constants for the constitutive equation

It can be concluded from the proposed constitutive equation shown in Eq. (4) that the flow stress is determined by the temperature compensation strain rate factor Z, materials constants A and α as well as the materials stress index n. While, the effect of deformation strain ε on true stress σ during hot deformation is not embodied. It is acknowledged that the materials constants Z, A, α and n will be changed because of the microstructure evolution of the materials during hot deformation process. There exists a functional relationship between the deformation strains and the material constants of the constitutive equation. Hence, by formulating the relationship between materials constants and

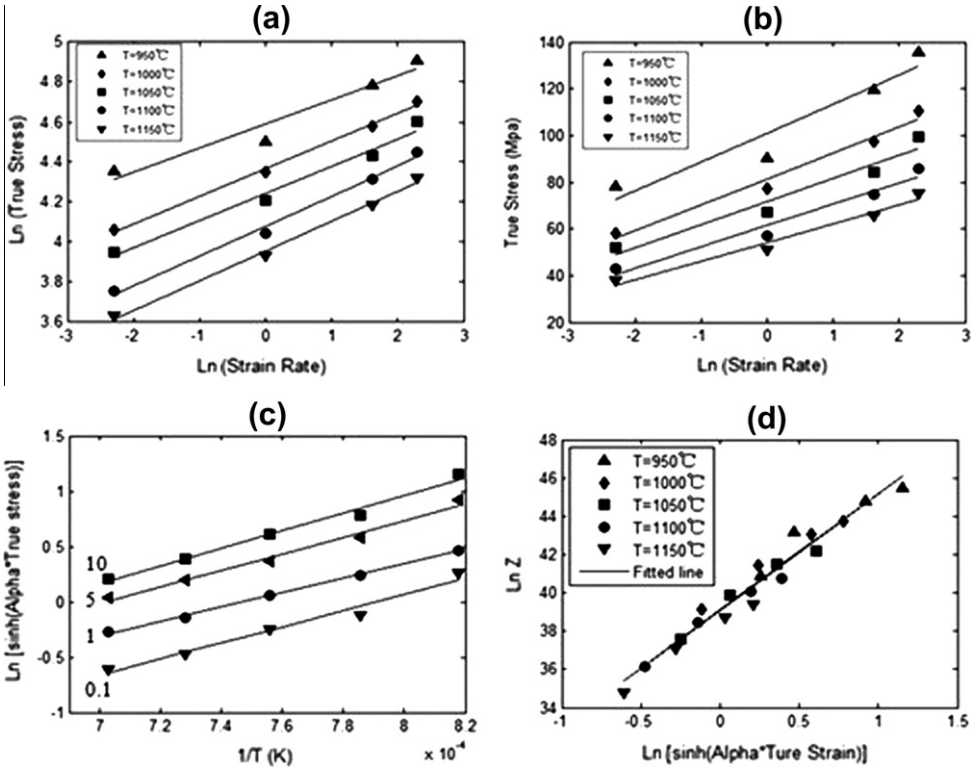

Fig. 5. (a) Relationship between ln $\dot{\varepsilon}$ and ln σ; (b) relationship between ln $\dot{\varepsilon}$ and σ; (c) relationship between $1/T$ and ln [sinh $(\alpha\sigma)$]; (d) relationship between ln [sinh $(\alpha\sigma)$] and ln Z.

deformation strain during hot deformation process, the relationship between true stress σ and true strain ε can be predicted by the proposed constitutive equation. The solution procedure for material constants under the deformation strain of 0.05 will be demonstrated as follows [20–22].

For the low stress level ($\alpha\sigma < 0.8$) and high stress level ($\alpha\sigma > 1.2$), relationship between flow stress and strain rate can be formulated in Eq. (5) and Eq. (6), respectively.

$$\dot{\varepsilon} = B_1\sigma^n \tag{5}$$

$$\dot{\varepsilon} = B_2 \exp(\beta\sigma) \tag{6}$$

where B_1, B_2 and β are the material constants, and $\alpha = \beta/n$.

Taking the logarithm of both sides of Eqs. (3) and (4), respectively, gives:

$$\ln\sigma = \frac{1}{n}\ln\dot{\varepsilon} - \frac{1}{n}\ln B_1 \tag{7}$$

$$\sigma = \frac{1}{\beta}\ln\dot{\varepsilon} - \frac{1}{\beta}\ln B_2 \tag{8}$$

By substituting the values of the flow stress and corresponding strain rate under the strain of 0.05 into Eqs. (7) and (8), it gives the relationship between the flow stress and strain rate. The value of n and β can be calculated from the slope of the lines in $\ln\dot{\varepsilon} - \ln\sigma$ and $\ln\dot{\varepsilon} - \sigma$ plots, respectively. Fig. 5a and b shows the $\ln\dot{\varepsilon} - \ln\sigma$ and $\ln\dot{\varepsilon} - \sigma$ plots under different deformation temperature, respectively. The slope of the lines under different temperature is approximately the same, the value of n and β can be obtained by linear fitting method. The mean value of n and β was computed as 7.2137 and 0.0924, respectively. And $\alpha = \beta/n = 0.01376$.

Table 2
Value of the material constants of GCr15 steel under different deformation strain.

Strain	Q (kJ/mol)	ln A (–)	n (–)	α (–)
0.05	438.69	39.08	7.21	0.013758
0.1	482.93	42.98	7.66	0.011941
0.15	507.74	45.23	7.95	0.011011
0.2	522.45	46.54	7.74	0.010611
0.25	497.18	44.18	7.05	0.010653
0.3	464.03	41.2	6.34	0.010763
0.35	437.94	38.88	5.87	0.010864
0.4	420	37.29	5.6	0.010942
0.45	401.78	35.69	5.37	0.010997
0.5	390.47	34.71	5.17	0.011102
0.55	381.33	33.91	5.06	0.011225
0.6	370.8	32.98	4.96	0.011360
0.65	363.06	32.32	4.89	0.011484

Eq. (9) can be obtained by taking the logarithm of both sides of Eq. (1). And for the given strain rate conditions, the activation energy of hot deformation Q can be calculated by differentiating Eq. (9).

$$\ln[\sinh(\alpha\sigma)] = \frac{1}{n}\left(\ln\dot{\varepsilon} + \frac{Q}{RT} - \ln A\right) \tag{9}$$

$$Q = Rn\frac{d\{\ln[\sinh(\alpha\sigma)]\}}{d(1/T)} \tag{10}$$

By substituting the values of temperature and flow stress that are obtained from a specified strain rate into Eq. (10), the value of Q can be calculated from the slope in the plot of $1/T - \ln[\sinh(\alpha\sigma)]$. Fig. 5c shows a group of parallel and straight lines representing the relationship between $1/T$ and $\ln[\sinh(\alpha\sigma)]$

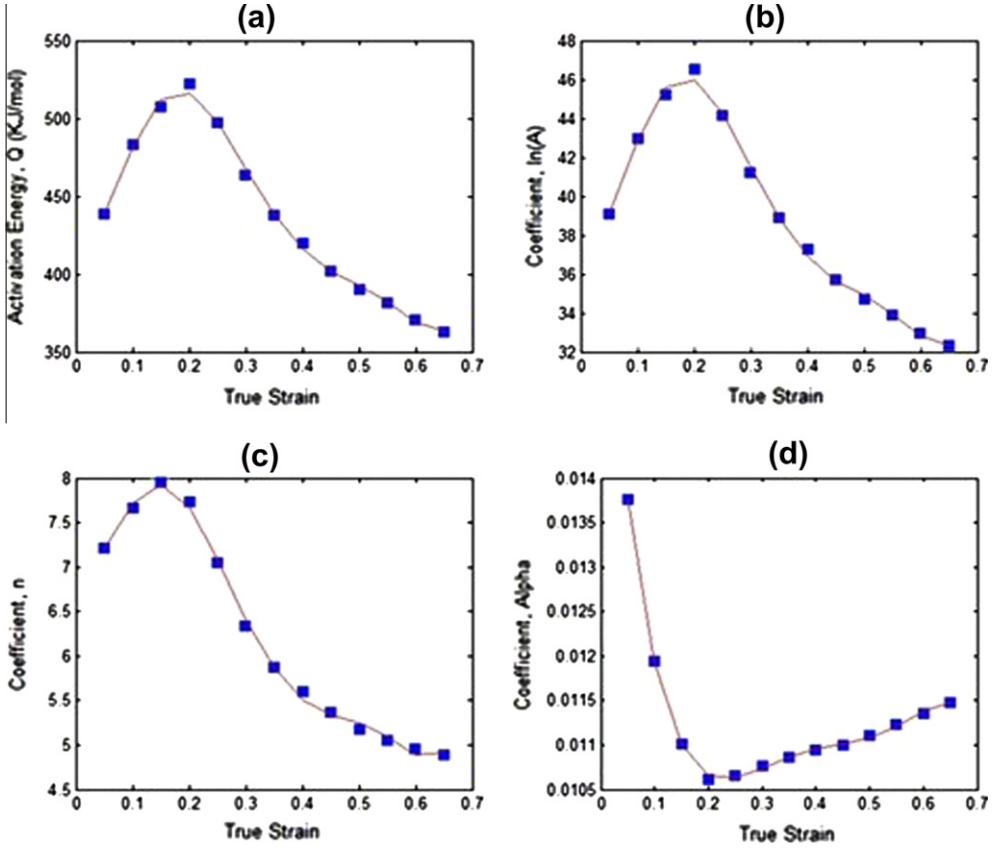

Fig. 6. Relationship between (a) Q; (b) $\ln A$; (c) n; (d) α and true strain by polynomial fit of GCr15 steel.

Table 3
Polynomial fitting results of Q, n, α and $\ln A$ of GCr15 steel. (x represents the undetermined coefficient of the polynomial fitting equations B, C, D and E).

	x_0	x_1	x_2	x_3	x_4	x_5	x_6
Q	423.583	−455.234	21531.98	−146442	396986.5	−486381	224414
n	6.91151	−3.98444	293.2812	−2320.49	6841.841	−8875.19	4274.923
α	0.016803	−0.07507	0.303931	−0.36561	−0.49674	1.526547	−0.96772
$\ln A$	37.93747	−48.5333	2019.52	−13622.3	36924.32	−45310.4	20947.74

at different strain rates. The value of Q can be evaluated as 438.69 kJ/mol by averaging the values of slope in the plot of $1/T - \ln[\sinh(\alpha\sigma)]$.

Eq. (11) can be obtained by taking the logarithm of both sides of Eq. (3).

$$\ln Z = n\ln[\sinh(\alpha\sigma)] + \ln A \tag{11}$$

It can be concluded from Eq. (11) that the value of $\ln A$ is the intercept of the plot $\ln[\sinh(\alpha\sigma)] - \ln Z$. By substituting the values of the experimental results under the strain of 0.05, relationship between $\ln[\sinh(\alpha\sigma)]$ and $\ln Z$ was obtained as shown in Fig. 5d. Then, the material constant A under the strain of 0.05 was calculated as 9.38e + 16 s^{-1}.

Using the same solve procedure, the values of material constants Q, $\ln A$, n and α of the constitutive equations were computed under different deformation strains within the range of 0.05–0.65 with the interval of 0.05. Table 2 shows the calculated values of the material constants under different deformation strain.

The relationships between Q, $\ln A$, n ,α and true strain for GCr15 steel (shown in Fig. 6) can be polynomial fitted by the compensation of strain, as shown in Eq. (12). The polynomial fitting results of Q, $\ln A$, n and α of GCr15steel are provided in Table 3. Fig. 6a–d shows the relationship between materials constants Q, $\ln A$, n , α and true strain by polynomial fit of GCr15 steel, respectively.

$$\begin{cases} Q = B_0 + B_1\varepsilon + B_2\varepsilon^2 + B_3\varepsilon^3 + B_4\varepsilon^4 + B_5\varepsilon^5 + B_6\varepsilon^6 \\ n = C_0 + C_1\varepsilon + C_2\varepsilon^2 + C_3\varepsilon^3 + C_4\varepsilon^4 + C_5\varepsilon^5 + C_6\varepsilon^6 \\ \alpha = D_0 + D_1\varepsilon + D_2\varepsilon^2 + D_3\varepsilon^3 + D_4\varepsilon^4 + D_5\varepsilon^5 + D_6\varepsilon^6 \\ \ln A = E_0 + E_1\varepsilon + E_2\varepsilon^2 + E_3\varepsilon^3 + E_4\varepsilon^4 + E_5\varepsilon^5 + E_6\varepsilon^6 \end{cases} \tag{12}$$

3.2.2. Modification of the Zener–Hollomon parameter

To verify the developed constitutive equation of GCr15 steel, comparison between the predicted and experimental results was carried out in this investigation. By applying the calculated material constants of the constitutive equation, the flow-stress values were predicted under different deformation temperatures of 950 °C, 1000 °C, 1050 °C, 1100 °C and 1150 °C with strain rates of 0.1 s^{-1},

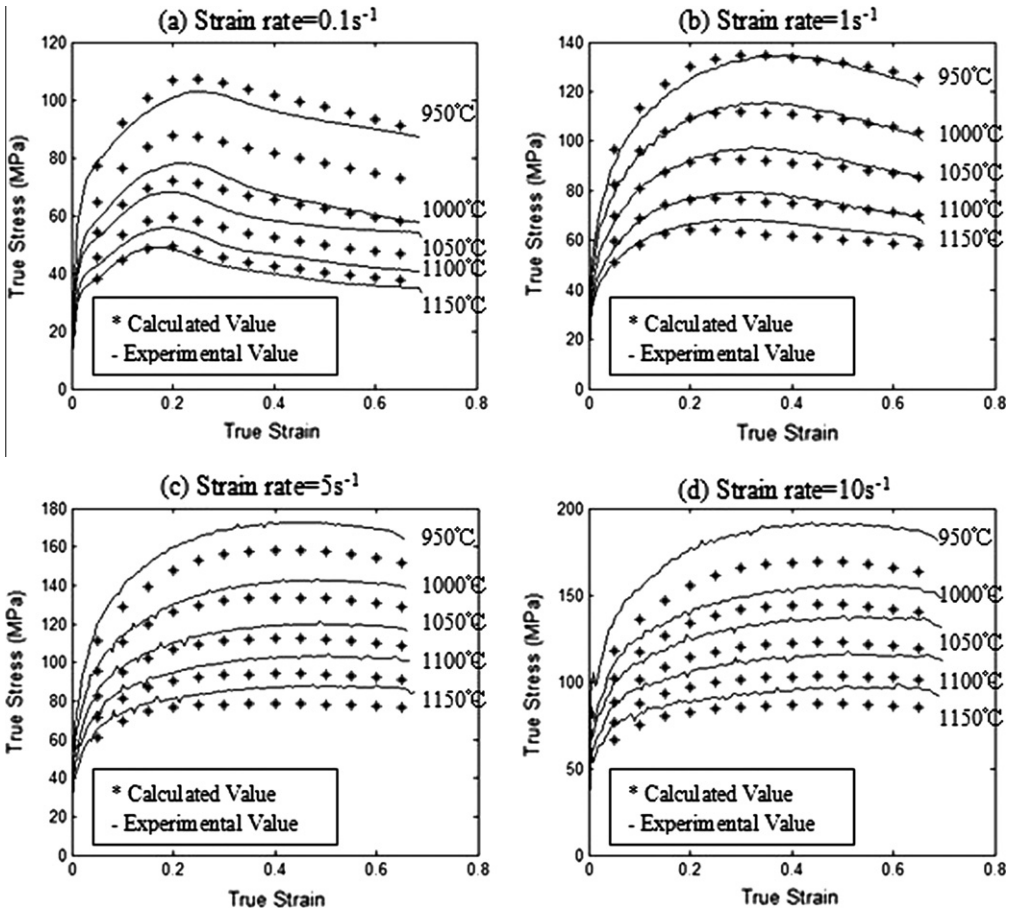

Fig. 7. Comparison between predicted and experimental flow stress curves of GCr15 steel under strain rates of: (a) 0.1 s^{-1}, (b) 1 s^{-1}, (c) 5 s^{-1} and (d) 10 s^{-1}.

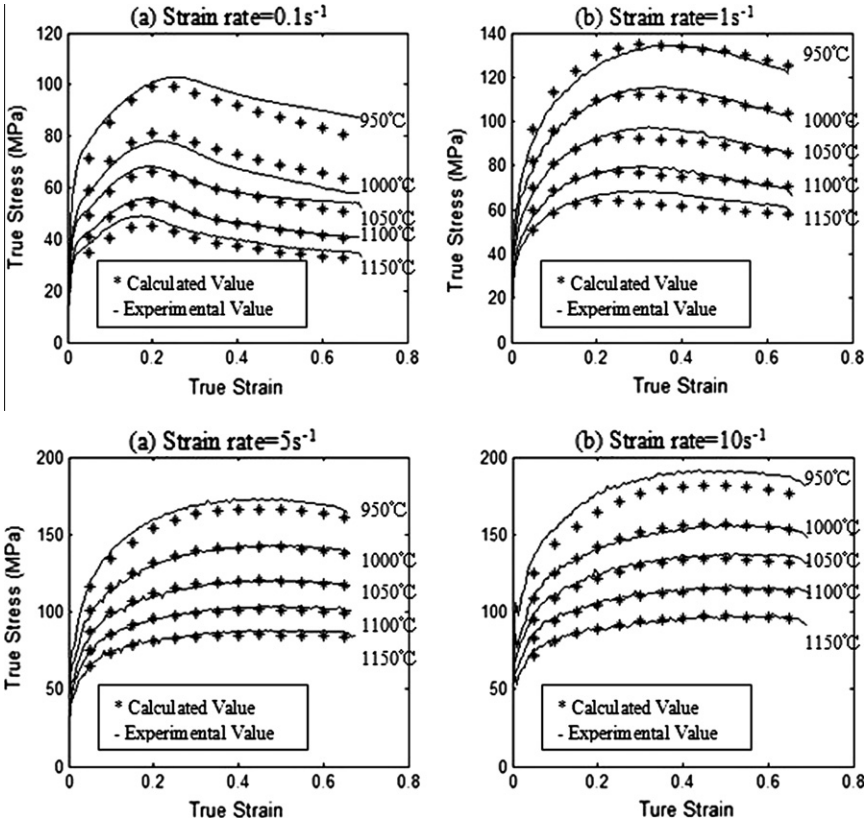

Fig. 8. Comparison between predicted flow stress values by modified constitutive equation and experimental flow stress curves of GCr15 steel under strain rates of: (a) 0.1 s^{-1}, (b) 1 s^{-1}, (c) 5 s^{-1} and (d) 10 s^{-1}.

1 s^{-1}, 5 s^{-1} and 10 s^{-1}. Fig. 7 shows the detailed comparison between predicted and experimental flow stress curves of GCr15 steel under strain rates of: (a) 0.1 s^{-1}, (b) 1 s^{-1}, (c) 5 s^{-1} and (d) 10 s^{-1}. It can be seen in Fig. 7b that the predicted flow stress of GCr15 shows a very good agreement with the experimental values at strain rate of 1. And it can be seen in Fig. 7a that the predicted flow stress value is larger than the experimental value at strain rate of 0.1 s^{-1}. Fig. 7c and d suggests that the predicted flow stress value is smaller than the experimental value at strain rate of 5 s^{-1} and 10 s^{-1}. Hence, it can be concluded from the analyzed results that the prediction accuracy of the developed constitutive equation can be improved by considering the compensation of strain rate.

In this investigation, a revised Zener–Hollomon parameter considering the compensation of strain rate was utilized to modify the constitutive equation of GCr15 steel. The revised Zener–Hollomon parameter (Z') was expressed as shown in Eq. (13). And the modified constitutive equation of GCr15 can be formulated as shown in Eq. (14).

$$Z' = \dot{\varepsilon}^{4/3} \exp\left(\frac{Q}{RT}\right) \tag{13}$$

$$\sigma = \frac{1}{\alpha} \ln\left\{\left(\frac{Z'}{A}\right)^{1/n} + \left[\left(\left(\frac{Z'}{A}\right)^{2/n} + 1\right)\right]^{1/2}\right\} \tag{14}$$

3.2.3. Verification of the constitutive equations

Fig. 8 shows the comparison between the experimental flow stress values and values predicted by the modified constitutive equation of GCr15 steel under different temperatures 950 °C, 1000 °C, 1050 °C, 1100 °C and 1150 °C with strain rate of 0.1 s^{-1}, 1 s^{-1}, 5 s^{-1} and 10 s^{-1}. It can be seen in Fig. 8 that the predicted flow stress values agree well with the experimental flow stress values.

In order to evaluate the accuracy of the developed constitutive equation, the predicted error δ between the predicted flow stress value (σ_P) and experimental flow stress value (σ_E) was calculated as the following equation:

$$\delta = \frac{\sigma_P - \sigma_E}{\sigma_E} \times 100\% \tag{15}$$

Table 4 shows the comparison between the predicted and experimental flow stress values at strain of 0.2, 0.4, 0.6 with strain rate of 0.1 s^{-1}, 1 s^{-1}, 5 s^{-1} and 10 s^{-1}. It can be seen in Table 4 that at strain rate of 0.1 s^{-1}, 1 s^{-1}, 5 s^{-1} and 10 s^{-1} the mean predictive error of the developed constitutive equation is −1.603%, −1.596%, −1.174% and −1.237%, respectively. The results indicate that the flow stress values predicted by the developed constitutive equation agree well with the experimental values, which confirms the accuracy and reliability of the proposed deformation constitutive equation of GCr15 steel.

4. Conclusions

In this paper, the thermal compressive deformation behavior of GCr15 was studied on the Gleeble-3500 thermo-simulation system over a practical rang of temperatures and strain rates. The following conclusions can be obtained:

Table 4
Comparison between the predicted (σ_P) and experimental (σ_E) flow stress values at strain of 0.2, 0.4, 0.6 with strain rate of 0.1 s^{-1}, 1 s^{-1}, 5 s^{-1} and 10 s^{-1}.

Strain rate $\dot{\varepsilon}$ (s^{-1})	Strain ε (–)	Temperature T (°C)	Experimental value σ_E (MPa)	Predicted value σ_P (MPa)	Error analysis	
					Error δ (%)	Mean error $\bar{\delta}$ (%)
0.1	0.2	950	100.8	99.09	−1.693	−1.603
		1000	77.76	80.90	4.040	
		1050	68.19	66.11	−3.046	
		1100	55.73	54.27	−2.627	
		1150	48.15	44.85	−6.859	
	0.4	950	96.165	91.82	−4.517	
		1000	67.402	72.90	8.160	
		1050	58.106	57.92	−0.319	
		1100	46.364	46.27	−0.208	
		1150	39.558	37.28	−5.771	
	0.6	950	89.79	82.93	−7.645	
		1000	59.88	65.51	9.404	
		1050	54.75	51.87	−5.267	
		1100	41.86	41.34	−1.242	
		1150	35.56	33.26	−6.457	
1	0.2	950	125.08	130.34	4.207	−1.596
		1000	108.76	109.38	0.568	
		1050	92.09	91.51	−0.630	
		1100	76.71	76.54	−0.224	
		1150	66.58	64.17	−3.626	
	0.4	950	134.33	133.81	−0.386	
		1000	114.6	110.78	−3.333	
		1050	95.76	91.18	−4.780	
		1100	77.56	74.87	−3.465	
		1150	66.73	61.55	−7.762	
	0.6	950	125.42	127.88	1.961	
		1000	105.11	105.83	0.687	
		1050	87.879	87.09	−0.894	
		1100	71.734	71.51	−0.308	
		1150	62.526	58.80	−5.962	
5	0.2	950	159.56	154.02	−3.474	−1.174
		1000	130.09	131.72	1.255	
		1050	109.89	112.20	2.105	
		1100	94.128	95.36	1.304	
		1150	81.3	81.02	−0.347	
	0.4	950	172.11	166.26	−3.400	
		1000	141.84	141.56	−0.195	
		1050	119.16	119.76	0.507	
		1100	101.83	100.83	−0.987	
		1150	86.913	84.65	−2.599	
	0.6	950	169.26	163.21	−3.573	
		1000	140.86	139.39	−1.043	
		1050	118.86	118.30	−0.471	
		1100	102.03	99.91	−2.081	
		1150	88.193	84.13	−4.606	
10	0.2	950	176.9	164.53	−6.991	−1.237
		1000	140.1	141.81	1.218	
		1050	125.38	121.72	−2.918	
		1100	105.11	104.19	−0.874	
		1150	87.89	89.09	1.367	
	0.4	950	189.51	180.68	−4.659	
		1000	151.43	155.52	2.702	
		1050	136.26	133.06	−2.348	
		1100	113.6	113.26	−0.300	
		1150	94.556	96.06	1.593	
	0.6	950	188.02	178.96	−4.819	
		1000	155.13	154.67	−0.295	
		1050	136.56	132.91	−2.671	
		1100	114.49	113.64	−0.744	
		1150	95.671	96.80	1.180	

(1) The flow stress of GCr15 steel during hot compressive process was recorded and the true stress–strain curves suggest that the stress level of GCr15 steel during hot compressive process decreases with increasing deformation temperature and decreasing strain rate.
(2) The optical micrograph of GCr15 steel after hot deformation process was observed and the existence of dynamic recrystallization austenitic grains indicates that the dynamic softening of GCr15 steel occurs during hot compression.
(3) The constitutive equation considering the compensation of strain rate during hot deformation could predict the flow stress throughout the entire temperature and strain rate ranges precisely.

Acknowledgements

This work was supported by the State Key Development Program for Basic Research of China (Grant No. 2011CB706605), the

General Program of National Natural Science Foundation of China (No. 50975215), the National Natural Science Foundation for Young Scientists of China (No. 51005171) and "the Fundamental Research Funds for the Central Universities (No. 125107002)". The authors would like to gratefully acknowledge the support from them.

References

[1] Han XH, Hua L. Plastic deformation behaviors of cold rotary forging under different contact patterns by 3D elastic–plastic FE method. Mater Trans 2009;50:1949–58.
[2] Deng XB, Hua L, Han XH, Song YL. Numerical and experimental investigation of cold rotary forging of a 20CrMnTi alloy spur bevel gear. Mater Des 2011;32:1376–89.
[3] Zhou G, Hua L, Qian DS, Shi DF, Li HX. Effects of axial rolls motions on radial–axial rolling process for large-scale alloy steel ring with 3D coupled thermo-mechanical FEA. Int J Mech Sci 2012;59:1–7.
[4] Zhou G, Hua L, Qian DS. 3D coupled thermo-mechanical FE analysis of roll size effects on the radial–axial ring rolling process. Comput Mater Sci 2011;50:911–24.
[5] Wang XK, Hua L. Analysis of guide modes in vertical hot ring rolling and their effects on the ring's dimensional precision using FE method. J Mech Sci Technol 2011;25:279–85.
[6] Luo J, Li MQ, Li XL, Shi YP. Constitutive model for high temperature deformation of titanium alloys using internal state variables. Mech Mater 2010;42:157–65.
[7] Mandal S, Rakesh V, Sivaprasad PV, et al. Constitutive equations to predict high temperature flow stress in a Ti-modified austenitic stainless steel. Mater Sci Eng A 2009;500:114–21.
[8] Samantaray D, Mandal S, Bhaduri AK, Venugopal S, Sivaprasad PV. Analysis and mathematical modelling of elevated temperature flow behaviour of austenitic stainless steels. Mater Sci Eng A 2011;528:1937–43.
[9] Lin YC, Chen MS, Zhong J. Constitutive modeling for elevated temperature flow behavior of 42CrMo steel. Comput Mater Sci 2008;42:470–7.
[10] Lin YC, Zhang J, Zhong J. Application of neural networks to predict the elevated temperature flow behavior of a low alloy steel. Comput Mater Sci 2008;43:752–8.
[11] Lin YC, Zhang J, Zhong J. Modeling of flow stress of 42CrMo steel under hot compression. Mater Sci Eng A 2009;499:88–92.
[12] Lin YC, Liu G. A new mathematical model for predicting flow stress of typical high-strength alloy steel at elevated high temperature. Comput Mater Sci 2010;48:54–8.
[13] Ding J, Kang GZ, Kan QH, Liu YJ. Constitutive model for uniaxial time-dependent ratcheting of 6061–T6 aluminum alloy. Comput Mater Sci 2012;57:67–72.
[14] Han YF, Zeng WD, Zhao YQ, Zhang XM, Sun Y, Ma X. Modeling of constitutive relationship of Ti–25V–15Cr–0.2Si alloy during hot deformation process by fuzzy-neural network. Mater Des 2010;31:4380–5.
[15] Gu SD, Zhang LW, Yue CX, et al. Multi-field coupled numerical simulation of microstructure evolution during the hot rolling process of GCr15 steel rod. Comput Mater Sci 2011;50:1951–7.
[16] Yue CX, Zhang LW, Liao SL, Gao HJ. Mathematical models for predicting the austenite grain size in hot working of GCr15 steel. Comput Mater Sci 2009;45:462–6.
[17] Yue CX, Zhang LW, Liao SL, et al. Research on the dynamic recrystallization behavior of GCr15 steel. Mater Sci Eng A 2009;499:177–81.
[18] Zencer C, Hollomon JH. Effect of strain rate upon plastic flow of steel. J Appl Phys 1944;15:22–32.
[19] Shi H, Mclaren AJ, Sellars CM, et al. Constitutive equations for high temperature flow stress of aluminum alloys. Mater Sci Eng 1997;13:210–6.
[20] Liang XP, Liu Y, Li HZ, Zhou CX, Xu GF. Constitutive relationship for high temperature deformation of powder metallurgy Ti–47Al–2Cr–2Nb–0.2W alloy. Mater Des 2012;37:40–7.
[21] Wu K, Liu GQ, Hu BF, Li F, Zhang YW, Tao Y, et al. Hot compressive deformation behavior of a new hot isostatically pressed Ni–Cr–Co based powder metallurgy superalloy. Mater Des 2011;32:1872–9.
[22] Changizian P, Zarei-Hanzaki A, Roostaei AA. The high temperature flow behavior modeling of AZ81 magnesium alloy considering strain effects. Mater Des 2012;39:384–9.